Phosphorus Adsorption onto an Industrial Acidified Laterite By–Product: Equilibrium and Thermodynamic Investigation

Phosphorus Adsorption onto an Industrial Acidified Laterite By–Product: Equilibrium and Thermodynamic Investigation

Journal:	*Asia-Pacific Journal of Chemical Engineering*
Manuscript ID:	APJ-14-0045
Wiley - Manuscript type:	Research Article
Date Submitted by the Author:	07-Feb-2014
Complete List of Authors:	Glocheux, Yoann; Queen's University of Belfast, School of Chemistry and Chemical Engineering Méndez Pasarín, Martin; Universitat Politècnica de Catalunya, Escola Tècnica Superior d'Enginyeria Industrial de Barcelona Albadarin, Ahmad B.; Queen's University of Belfast, School of Chemistry and Chemical Engineering Mangwandi, Chirangano; Queen's University of Belfast, School of Chemistry and Chemical Engineering Chazarenc, Florent; L'UNAM Université, Ecole des Mines de Nantes Walker, Gavin; University of Limerick, Department of Chemical and Environmental Sciences; Queen's University of Belfast, School of Chemistry and Chemical Engineering
Keywords:	Phosphorus, Laterite, Adsorption, Thermodynamic, Ferric Aluminium Sulphate

Phosphorus Adsorption onto an Industrial Acidified Laterite By–Product: Equilibrium and Thermodynamic Investigation

Yoann Glocheux[1]*, Martin Méndez Pasarín[1,2], Ahmad B. Albadarin[1], Chirangano Mangwandi[1], Florent Chazarenc[3] and Gavin M. Walker[1,4]

[1] School of Chemistry and Chemical Engineering, Queen's University Belfast, United Kingdom

[2] Escola Tècnica Superior d'Enginyeria Industrial de Barcelona, Universitat Politècnica de Catalunya, Spain

[3] L'UNAM Université, École des Mines de Nantes, CNRS, GEPEA, UMR 6144, 4 rue Alfred Kastler, B.P. 20722, F–44307 Nantes Cedex 3, France

[4] Materials Surface Science Institute, Department of Chemical and Environmental Sciences, University of Limerick, Ireland

*Corresponding author

Tel: +44 (0) 2890 974253

Fax: +44 (0) 2890 974627

E–mail: yglocheux01@qub.ac.uk

Abstract (200 words)

The present research investigates the uptake of phosphate ions from aqueous solutions using Acidified Laterite, a by–product from the production of Ferric Aluminium Sulphate using Laterite. Phosphate adsorption experiments were performed in batch systems to determine the amount of phosphate adsorbed as a function of solution pH, adsorbent dosage and thermodynamic parameters per fixed P concentration. Kinetic studies were also carried out to study the effect of adsorbent particle sizes. The maximum removal capacity of ALS observed at pH 5 was 3.68 mg $P.g^{-1}$. It was found that as the adsorbent dosage increases, the equilibrium pH decreases, so an adsorbent dosage of 1.0 $g.L^{-1}$ of ALS was selected. Adsorption capacity (q_m) calculated from the Langmuir isotherm was found to be 2.73 $mg.g^{-1}$. Kinetic experimental data were mathematically well described using the pseudo first order model over the full range of the adsorbent particle size. The adsorption reactions were endothermic and the process of adsorption was favoured at high temperature, the ΔG and ΔH values implied that the main adsorption mechanism of P onto ALS is physisorption. The desorption studies indicated the need to consider a NaOH 0.1 M solution as an optimal solution for practical regeneration applications.

Keywords: Laterite; Phosphorus; Adsorption; Thermodynamic; Ferric Aluminium Sulphate

1 Introduction

The presence of high phosphate levels alongside a high level of nitrate in rivers and lakes is responsible for the eutrophication phenomenon. Lakes and rivers are usually considered eutrophic for P level between 0.035 to 0.1 $mg.L^{-1}$ and hypereutrophic for levels higher than 0.1 $mg.L^{-1}$ [1]. Environments with phosphorus levels between 0.010 $mg.L^{-1}$ and 0.035 $mg.L^{-1}$ are considered mesotrophic toward this element, i.e. its concentration level is optimal for the development of a balanced ecosystem. Nevertheless, due to an increase in the human activity, the level of phosphorous in water bodies has increased considerably in the past decades. Levels of phosphorous as high as 0.675 $mg.L^{-1}$ were noticed in Northern Ireland in Lough Egish for example, [2]. The nature of the input of phosphate from the environment into rivers and lakes is either diffused, like agriculture, or the source can be concentrated like wastewater treatment plant discharge points. The European Urban Waste Water Treatment Directive (EUWWTD) limits the phosphorus discharge level to 1 $mg.L^{-1}$ for installation larger than 100000 Population Equivalent or 2 $mg.L^{-1}$ for installation between 10000 and 100000 PE, moreover the treatment efficiency has to be equal to or higher than 80 % removal [3].

The difficulty in implementing the EUWWTD on a small scale waste water treatment plant and the input of phosphorus from diffuse sources requires the development of low cost and simple phosphorus adsorption techniques to enhance the control of P levels in rivers and water bodies.

The use of cheap ore and natural materials for the adsorption of P from water has been regarded as a good strategy in decreasing the phosphorus level below 0.035 $mg.L^{-1}$. A number of studies have tested the phosphorus adsorption capacity of different materials like: limestone, dolomite, Laterite or even half burn limestone, and removal capacities ranging from 0.02 to 20 $mg.g^{-1}$ were reported [4]. Industrial by–products have also been successfully utilized as P adsorbents, such as; red mud generated during the production of aluminium, blast furnace generated during the production of steel or residual iron and aluminium oxides from WWTPs [5-8].

The review by Vohla *et al.* on the use of adsorbents for P removal in wetland type systems differentiated three types of materials: natural material, industrial by–product and manmade sorbents, [9]. According to the report, industrial by–products can have a very high removal capacity, up to 420 $mg.g^{-1}$, natural materials showed a maximum P adsorption capacity of 40 $mg.g^{-1}$ and finally man–made materials displayed a maximum removal of 12 $mg.g^{-1}$ [9]. The

adsorption capacity is usually very sensitive to pH and the authors also showed that the content of CaO has a positive effect on the general adsorption of P. Acidified Laterite by Sulphuric acid (ALS) waste material generated during the production of Ferric Aluminium Sulphate showed very promising results as an arsenic adsorbent for drinking water purification applications [10]. As both phosphate and arsenate are anions with similar pKa and chemical structure, it is expected that ALS material can efficiently remove P as phosphate from water. In the present study, the use of ALS by–product for the elimination of P from aqueous solutions was explored under batch conditions. As the study is focusing on the removal of phosphorus as phosphate onto ALS, raw Laterite was used at the beginning to quantify the improvement between the raw and acidified lateritic material. The effects of solution pH, adsorbent dose and temperature on the adsorption process were examined. The possibility to use the ALS material in a wetland type system or in a packed bed system for polishing compact WWTP effluent relies on its capacity to decrease P levels below 0.035 $mg.L^{-1}$. It is thus important to describe the adsorption mechanism involved in P fixation onto ALS. This study also describes the diffusion of P molecules inside the material pores, as this feature will greatly impact the adsorption capacity of the material in dynamic conditions.

2 Materials and methods

2.1 Lateritic materials

Laterite is a naturally occurring ore rich in aluminium, iron, silica and titanium oxides [11]. The Acidified Laterite by–product used in this study to adsorb phosphate is an industrial waste produced during the manufacture of Ferric Aluminium Sulphate (FAS). During the industrial process iron and aluminium are extracted from Laterite using a solution of sulphuric acid at 70 °C. The Acidified Laterite (ALS) used is this work has been in contact with sulphuric acid, leaving a significant amount of sulphate surface groups which have a positive effect on anion adsorption [10]. The raw Laterite received is mined in Ballymena (NI) by Stevenson Quarries LTD and the ALS material is produced by Clinty Chemicals LTD in the same location. The samples were dried for 24 h at 60 °C, sieved in three different particle sizes: lower than 75 µm, 500 – 600 µm and 1000 – 1180 µm and the samples were conserved in vacuum desiccators. The two lateritic samples were extensively characterized in a previous study [10]. Noticeable physical–chemical characteristics of the ALS sample are: a surface area of 98.48 $m^2.g^{-1}$; BET porosity around 0.2 $cm^3.g^{-1}$; a point of zero charge of 5.1 and the presence of sulphate groups on the surface of the sample. Further analytical

techniques were used to identify the crystal composition of the oxides present in the ALS sample as well as in the raw Laterite.

2.2 Adsorbent characterization

2.2.1 XRD X–Ray Diffraction analysis

An XRD analysis was carried out to determine the crystalline nature of the main oxides present in the two lateritic samples. The XRD equipment used to carry out the crystal identification in the samples is a PANalytical X'pert model from Philips. Radiation was carried out by a Cu K–alpha 1 lamp at wavelength 0.154056 nm. Fully quantitative analysis was carried out using the X'pert analytical tool and database.

XRD results were coupled with XFR results in order to tune the quantification of the main oxides present in the samples. XRF analysis was carried out using an Axios Advanced analyser from PANalytical and results were discussed previously [10].

2.2.2 FTIR Fourier Transformation Infra–Red spectrophotometry

Untreated ALS and ALS after saturation with phosphate solution were analysed by FTIR. Samples in equilibrium for 48 h with P solutions of 1, 10 and 100 $mg.L^{-1}$ of phosphorus at pH 7 were studied. The KBr tableting method was used and samples were analysed using a PerkinElmer Spectrum One FT–IR spectrometer instrument.

2.3 Characterisation of P adsorption in batch and column experiments

2.3.1 Chemicals and water solutions

Chemicals of at least reagent grade were used as received from Sigma Aldrich. Deionised water was used in all experiments and provided by an ELGA Maxima ultrapure water system; resistivity of 18.2 MΩ.cm 100 $mg.L^{-1}$ phosphorus stock solutions were produced by dissolving corresponding amounts of sodium di–hydrogen phosphate salts and were diluted for subsequent experiments. All solutions were buffered with 100 $mg.L^{-1}$ of $NaHCO_3$ and pHs were adjusted by adding dilute solutions of HCl or NaOH. pHs were recorded by the means of a pH Thermo Scientific Orion 3 Star pH meter equipped with a Camlab pH probe calibrated with 3 standard solutions at pH 4.01; 7.00 and 10.00.

2.3.2 Dose study

Initial concentration of phosphorus in the adsorbent dosage study was set at 25 $mg.L^{-1}$ and the pH was maintained around 7. Adsorbent dosages ranging from 1 to 10 $g.L^{-1}$ were tested

in removing phosphorus. Experiments were carried out in 50 mL glass jars and allowed to reach equilibrium during 72 h onto a horizontal shaker at 100 rpm.

2.3.3 pH study

pH studies were performed in the same way as dosage studies excepted that the dosage was set at 1 $g.L^{-1}$and initial pHs were adjusted from 3 to 10. pH values at equilibrium were recorded and used to study the effect of pH on the P adsorption capacity of ALS. Equilibrium time was 72 h.

2.3.4 Isotherm analysis

The isotherm of P adsorption onto ALS was studied using phosphate solutions ranging from 5 to 50 $mg.L^{-1}$. Dosage of material was set at 1 $g.L^{-1}$ and pH maintained around 7. Equilibrium time was 72 h.

2.3.5 Kinetics of adsorption and effect of particle size

Kinetic removal of P by ALS and raw Laterite was carried out in 1 L beakers using 1L solution at 25 $mg.L^{-1}$ P and pH 7. Adsorbent dosage was 1 $g.L^{-1}$ and different particle sizes of adsorbent were tested: diameter of 1000 – 1180 µm; 500 – 600 µm and < 75 µm. Solutions were completely mixed using magnetic stirrers set at 300 rpm. Stainless steel 100 mesh buckets were used in order to prevent any size variation during the experiments aided by the crushing down of the materials with magnets. When a stainless steel bucket was used alone no P adsorption onto the bucket was observed.

2.3.6 Thermodynamic investigation

The effect of temperature on the adsorption of phosphorus by ALS was studied. P adsorption isotherm experiments were carried out at 4 different temperatures: 298, 303, 313 and 323 K. The experimental procedure followed was the same as the one used for the isotherm room temperature of 298 K. For isotherms studied at higher temperatures, glass jars were shaken at 100 rpm in a thermo–regulated shaken bath Clifton NE5–28D for 72 h.

2.4 Concentration Analysis

A colorimetric method was used to measure the phosphorus concentration. All samples from the present batch experiments were analysed by the colorimetric molybdenum blue method. The method presented by Tsang *et al.* was followed for phosphorus measurement only, with the addition of minor changes [12]. The calibration curve was set to phosphorus instead of phosphate using a certified 1000 $mg.L^{-1}$ P solution from Alfa Aesar and the procedure was

downscaled to a 10 mL sample. A few samples were also analysed by ICP–OES for P and S at 178.2 and 182.0 nm respectively to ascertain the results obtained by the colorimetric method. An ICP–OES Thermo Scientific IRIS Intrepid was used in that case. Very good linear regression was obtained for the calibration of the colorimetric molybdenum blue method, $r^2 > 0.99$ for 7 calibration points over the range 1 to 5 mg.L^{-1}.

After adsorption experiments and prior to any analysis, samples were filtered using 13 µm cut off cellulose acetate filters and acidified at 2 % HNO_3, only in the case of ICP analysis. When powder adsorbents were used, i.e. materials having a particle size lower than 75 µm, samples were centrifuged at 5300 rpm before analysis.

2.5 Mathematical modelling

Mathematical modelling was used to interpret data obtained in the experiments. The isotherm, kinetic and column model constants were determined using Sigma Plot and the non–linear models are presented in the following sections.

2.5.1 Isotherms modelling

Batch studies results were modelled using Langmuir and Freundlich adsorption models presented by equations (1) and (2) respectively [13].

Langmuir model:

$$q_e = \frac{q_m b_L C_e}{1 + b_L C_e} \quad (1)$$

Freundlich model:

$$q_e = K_F C_e^{\,n} \quad (2)$$

Where q_e is the amount of pollutant adsorbed at equilibrium for a given initial concentration in mg.g^{-1}. q_m is the maximum amount of pollutant adsorbed at equilibrium in mg.g^{-1}. C_e is the concentration of phosphorus in the bulk solution at equilibrium in mg.L^{-1}. b_L is the Langmuir constant in L.mg^{-1}. K_F is the Freundlich coefficient in mg^{1-n}.g^{-1}.L^{n}. n is the Freundlich equation constant and is dimensionless.

Isotherms obtained at different temperatures were modelled using the Temkin isotherm usually represented by equation (3) [14] and [15].

$$q_\theta = \frac{RT}{b_T} \ln\left(K_T C_e\right) = B_T \ln\left(K_T C_e\right) \quad (3)$$

Where q_θ is the percentage coverage of the adsorbent. R is the ideal gas constant in J.mol^{-1}.K^{-1}, T the temperature in K, b_T is the Temkin constant expressed in J.mol^{-1} and is linked to the heat of adsorption and finally K_T in L.mg^{-1} is the Temkin equilibrium binding constant.

The Dubinin–Radushkevich (DR) model was originally developed to describe the physical adsorption onto homogeneous microporous media following a pore filling process [16]. It has been applied to many other adsorption mechanisms and it is usually used to differentiate between physical and chemical adsorption phenomenon. Equation (4) presents the common DR isotherm form with equation (5) calculating the variable ε_{DR}. Equation (6) presents the calculation of E, the mean free energy of adsorption of the process model expressed in kJ.mol^{-1} [17].

$$q_e = q_s \times e^{\left(-k_{ad}\varepsilon_{RD}{}^2\right)} \quad (4)$$

$$\varepsilon_{RD} = RT \ln\left(1 + \frac{1}{C_e}\right) \quad (5)$$

$$E = \frac{1}{\sqrt{2B_{DR}}} = \frac{1}{\sqrt{2k_{ad}}} \quad (6)$$

Where q_s is the theoretical isotherm saturation capacity in mg.g^{-1}; k_{ad} is the DR isotherm constant in mol^2.J^{-2}; ε_{DR} is the DR isotherm variable in J.mol^{-1}; B_{DR} is the DR isotherm constant k_{ad} and E is the adsorption energy expressed in J.mol^{-1}.

From the literature, it has been reported that generally the adsorption process can be distinguished based on the free energy of binding, as chemisorption shows higher activation energy than physisorption. The following classification is generally used, [18]:

- Physisorption processes have adsorption energies < 40 kJ.mol^{-1}
- Chemisorption processes have adsorption energies > 40 kJ.mol^{-1}
- Chemical ion exchange processes have adsorption energies between 8.0 and 16 kJ.mol^{-1}
- Adsorption is physical in nature if adsorption energies are < 8.0 kJ.mol^{-1}

2.5.2 Kinetics modelling

The pseudo first and pseudo second order models were applied to kinetics experiments using equations (7) and (8) which are integrated forms of these two models.

Pseudo first order model [19]:

$$\ln\left[\frac{q_e - q_t}{q_e}\right] = -k_1 t \quad (7)$$

Pseudo second order model [20]:

$$\frac{1}{(q_e - q_t)} = \frac{1}{q_e} + k_2 t \quad (8)$$

Where q_t is the amount of pollutant adsorbed at time t in mg.g^{-1}. k_1 is the pseudo–first order kinetic constant in min^{-1}. k_2 is the pseudo second order kinetic constant in g.mg^{-1}.min^{-1}.

2.5.3 Thermodynamic modelling

Studying the thermodynamic behaviour of adsorption reactions can reveal useful information about the nature and characteristic of the occurring reaction. The Gibbs free energy ΔG° can be expressed by equation (9), [21].

$$\Delta G^o = -RT\ln K_o \quad (9)$$

Where K_0 is the apparent equilibrium constant from the adsorption reactions modelled by a simple equilibrium equation as expressed by equation (10), [22].

$$M_{sol} + S \equiv \leftrightarrow S \equiv M \quad (10)$$

K_0 is calculated as follows by equation (11).

$$K_o = \frac{[S \equiv M]_a}{[M_{sol}]_a} \quad (11)$$

With $[S{\equiv}M]_a$ and $[M_{sol}]_a$ expressed as activity. In dilute systems, concentration can be used to approximate activities [23] and K_o can be expressed at low concentrations as shown in equation (12).

$$K_o \approx \frac{q_e}{C_e} \quad (12)$$

K_0 can be calculated using the $\ln(q_e/C_e)$ value obtained when q_e approaches zero [1]. There are also different ways to measure K_o present in the literature using either the Freundlich, Langmuir or Temkin equilibrium constant [14, 24, 25]. Entropy and enthalpy of adsorption can be obtained using the following Gibbs free energy definition presented in equation (13).

$$\Delta G^0 = \Delta H^0 - T\Delta S^0 \quad (13)$$

These parameters can also be obtained by the rearranged equation (14), [23].

$$\ln K_0 = \frac{\Delta S^0}{R} - \frac{\Delta H^0}{RT} \quad (14)$$

2.5.4 Diffusion modelling

2.5.4.1 Intraparticle diffusion modelling

The intraparticle model links the adsorbed quantity of pollutant at a given time with the time t by equation (15) [26].

$$q_t = k_{id} t^{0.5} \quad (15)$$

Where the intraparticle diffusion rate k_{id} is constant and is expressed in $mg.g^{-1}.h^{-0.5}$. k_{id1} represents the intraparticle diffusion coefficient of the diffusion phase 1. If the plot of q_t versus $t^{0.5}$ is linear then it means that the intraparticle diffusion is the limiting step in the experimental conditions. The intraparticle diffusion rate is generally constant over a period of time at initial condition only.

2.5.4.2 Boyd diffusion model

Boyd diffusion model is also a single resistance model and can be expressed by the equation (16), [27].

$$\frac{q_t}{q_e} = 1 - \left(\frac{6}{\pi^2}\right)\sum_{n=1}^{\infty}\left(\frac{1}{n^2}\right)\exp\left(-n^2 B \times t\right) \quad (16)$$

Where B is a coefficient expressed in h^{-1}. Equation (16) can be approximated by the following equations (17) and (18) based on Reichenberg work [28].

If $q_t/q_e > 0.85$ then

$$B \times t = 0.4977 - \ln\left(1 - \frac{q_t}{q_e}\right) \quad (17)$$

If $q_t/q_e < 0.85$ then

$$B \times t = \left(\sqrt{\pi} - \sqrt{\pi - \left(\frac{\pi^2 \frac{q_t}{q_e}}{3}\right)}\right)^2 \quad (18)$$

An effective diffusion coefficient can then be calculated from B by the following equation (19) presented by Reichenberg [28].

$$B = \frac{\pi^2 \times D_{eff}}{r^2} \quad (19)$$

Where r is the particle radius of the adsorbent. If the plot of $B \times t$ versus t is a straight line passing through the origin then the main resistance is due to intraparticle diffusion and $D_{eff} = D_{intra}$ [27].

Based on unit integrity, the Boyd coefficient can also be approximated using equation (20).

$$B \approx \left(\frac{k_{id1}}{q_e} \right)^2 \quad (20)$$

Where k_{id1} is the intraparticle constant in $mg.g.h^{-0.5}$, q_e is the equilibrium sorbed pollutant determined by a kinetic model and expressed in $mg.g^{-1}$. Equation (20) allows the use of intraparticle model coefficients to calculate intraparticle diffusion coefficients.

3 Results and discussion

3.1 Crystalline structure of Laterite and ALS and their chemical composition

Raw Laterite and ALS were previously analysed by XRF and the results were presented earlier [10]. The two samples have been categorised as lateritic samples because of their respective $SiO_2/(Fe_2O_3+Al_2O_3)$ ratio [29]. The Laterite mined showed a high level of aluminium oxides and iron oxides compared to the ALS which was assigned to the acid extraction process.

XRD spectrum of both raw Laterite and ALS are presented in Figure 1. The samples are natural samples and full identification of crystals is limited because of impurities and the possible presence of amorphous phases.

Figure 1 XRD spectrum of Laterite and ALS samples and main crystals phases identified

Five main crystal phases were identified and the corresponding full quantitative analysis results are presented in Table 1. The XRD fully quantitative analysis was coupled with the XRF results obtained previously to fine tune the crystal quantification.

Table 1 XRD analysis of raw Laterite and ALS samples. Results are expressed in % w/w

The two main crystal phases identified in Laterite are gibbsite and kaolinite which are characteristic of Laterite mined in Northern Ireland [11]. Upon sulphuric acid treatment Kaolinite content remains very high. Ratios of both iron and aluminium crystals to silica crystals decrease which underlines the dissolution of these targeted metal oxides and hydroxides. When XRF and XRD analysis results were compared, differences were noticed, mainly assigned to the Lost On Ignition (LOI) during XRF analysis and the presence of amorphous crystal phases in XRD fully quantitative analysis.

3.2 Effect of material dosage onto P adsorption

Different material ratios were used to study the effect of adsorbent dosage and results are presented in Figure 2. It can be noticed that a dosage of 8 $g.L^{-1}$ is necessary to completely remove the initial 25 $mg.L^{-1}$ of phosphorus and that only 10 % of P removal is reached when 1 $g.L^{-1}$ of adsorbent is used. It is interesting to note that the P removal percentage increases nearly constantly from 10 % at 1 $g.L^{-1}$ of adsorbent to almost 100 % at 8 $g.L^{-1}$.

The other noticeable result is the effect of adsorbent dosage on the equilibrium solution pH. The pH decreases when the adsorbent dosage is increased; this is linked to the residual acidic groups present in the material. As more ALS is used in the adsorption study the pH is decreased and can in return affect the P adsorption performance of the material. In the present study P is removed more favourably at low pH. Indeed as the dosage increases, the pH decreases and the average P adsorption capacity increases from 2.6 to 3.2 $mg.g^{-1}$ before dropping down when the total P removal percentage reaches 100 %, as seen in Figure 2. The effect of the pH explains the pattern noticed in the dose study as it is very rare to obtain a constant increase in the adsorption capacity of a material in the function of a dosage increase. In order to minimize the pH change due to ALS addition, a dosage of 1 $g.L^{-1}$ of ALS was selected for subsequent experiments.

Figure 2 Phosphorus removal by increasing ALS dosage ratio; $[P]_0 \approx 25$ $mg.L^{-1}$; pH_0 is 7

3.3 pH effect onto P removal by ALS

The effect of pH on phosphorus adsorption was studied using a solution of 25 $mg.L^{-1}$ of phosphorus to prevent total removal of P from the solution. Results are displayed in Figure 3. It can be seen that pH 5 is the optimal pH for phosphorus removal using ALS. The maximum removal capacity of ALS observed at pH 5 is 3.68 mg $P.g^{-1}$ which corresponds to more than a 50 % increase in P removal compared to results obtained at pH 7.

Figure 3 Phosphorus adsorption study in function of pH at equilibrium. $[P]_0 \approx 25$ mg.L^{-1}

The Point of Zero Charge (PZC) of ALS was previously evaluated at 5.1 [10] and explains the pattern of the plot observed in Figure 3. At pH lower than the PZC, the lateritic by–product is positively charged thus attracting anions. As it can be seen in Figure 4, at pH lower than 5.1, phosphorus is mainly present in the solution as dihydrogen phosphate, $H_2PO_3^-$, explaining the good removal of phosphorus. At pH higher than the PZC the maximum P removal capacity of ALS decreases as the phosphorus specie are becoming more negative. On the other hand, for a pH lower than the PZC, the ALS phosphorous adsorption capacity slowly decreased as the phosphorous species present in the solution are neutrally charged. The strong effect of pH on the adsorption of phosphorus onto ALS suggests an adsorption process mainly controlled by physisorption [30]. At lower pH, the effect of pH is decreasing which can indicate the prevalence of another adsorption process like ion–exchange [31].

Figure 4 Phosphorous speciation diagram and PZC of the lateritic by–product ALS

3.4 Isotherms of P adsorption by ALS

Results of the concentration study of phosphorous adsorption onto ALS and the resulting isotherms are presented in Figure 5. Data points were fitted with both Freundlich and Langmuir models.

Figure 5 Isotherm modelling of phosphorus adsorption onto ALS. ALS particle size is lower than 75 µm and $pH_e \approx$ 7.0

It can be observed from Table 2 that the Freundlich model presents the better correlation value to the experimental points obtained. It should be noticed that the lack of data points at low concentration does not allow a full comparison of the Langmuir and Freundlich models. Nevertheless as C_e increases, q_e gradually increases over the concentration range studied. The absence of a strict plateau is a feature indicative of a process following the Freundlich model [32].

Table 2 Isotherm models parameters and correlation coefficient of P adsorpiton onto ALS

The phosphorous maximum adsorption capacity q_m of ALS was evaluated at 2.73 mg $P.g^{-1}$ or 0.090 mmol $P.g^{-1}$ over the concentration range studied. This value is significantly higher than the As(V) removal capacity of the same material revealed as 0.027 mmol $P.g^{-1}$ [10]. The higher concentration range used in this study can explain this difference as adsorption mechanisms are expected to be similar due to the close chemical structure of arsenate and phosphate.

Additionally the q_e value of ALS at 10 $mg.L^{-1}$ reaches 2.5 mg $P.g^{-1}$ which can be considered a high removal capacity for a by–product when compared to data from literature as presented in Table 3.

Table 3 Comparison of P adsorption capacities of ALS and reported results from the literature

Moreover it is interesting to note that the P removal capacity of ALS is evaluated at 2.19 $mg.g^{-1}$ at 2 $mg.L^{-1}$, 2.09 $mg.g^{-1}$ at 1 $mg.L^{-1}$ and 1.65 $mg.g^{-1}$ at 0.035 $mg.L^{-1}$. The adsorption capacity of the material is very good at low concentrations.

3.5 Thermodynamic investigation of P adsorption onto ALS

The impact of temperature on the P adsorption capacity helps to describe the reaction occurring during the P accumulation onto ALS. Figure 6 shows that the adsorption of phosphorous onto ALS increases as the temperature increases. This is characteristic of endothermic reactions as the heat provided shifts the reaction equilibrium. The q_{max} for phosphorus adsorption onto ALS increased from 2.74 to 3.24 mg.g^{-1} with the increase in temperature from 298 to 323 K. This is attributed to both the enlargement of the pore size and the formation of new adsorption sites [33]. Isotherms at different temperatures were fitted to the Temkin model as presented in Figure 6.

Figure 6 P adsorption isotherms obtained at different temperatures modelled using Temkin isotherm mathematical model

The Temkin isotherms show an inverse order at very low concentrations in relation to the experiment temperature when compared to the order noticed at higher concentrations. This is probably due to the low adsorption capacity of the material and the lack of data points over this range. Because of this pattern the use of the Temkin, Langmuir or Freundlich constants to calculate K_0 gave an erroneous solution to equation (12), i.e. a negative enthalpy. Indeed K_0 was calculated using the $\ln(q_e/C_e)$ value obtained when q_e approaches zero [21]. To overcome this difficulty, equation (21) was used to calculate K_0 [24] and [34].

$$K_0 \approx 1000 \times \frac{q_e}{C_e} \qquad (21)$$

K_0 is dimensionless as explained by Milonjic and unit integrity as to be respected [25]. This explains the presence of the 10^3 factor before q_e/C_e which is expressed in L.g^{-1}. From the plot of equation (13); i.e. $\ln K_o$ *vs. 1/T*; the values of ΔH and ΔS can be determined from the slope and intercept respectively. The results obtained are presented below in Table 4 and the linear dependency of the free energy of Gibbs to temperature is shown in Figure 7.

Table 4 Free energy of Gibbs, enthalpy and entropy of P adsorption onto ALS

The negative ΔG value indicates a spontaneous reaction of P adsorption onto ALS. The positive enthalpy ΔH proves that the reaction is endothermic as suggested by the isotherm plot. The positive value of ΔS shows that the entropy, often attributed to the randomness of

the system, increases in the reaction of adsorption, i.e. at the liquid–solid surface [35]. This shows the favourable nature of the reaction, even if the low value limits the interpretation [14]. ΔG value of around –10 kJ.mol^{-1} and a low enthalpy of around 5.5 kJ.mol^{-1} suggest that physisorption is the main mechanism involved in the adsorption of P onto ALS. Chemisorption usually displays a high bonding strength with the ΔH value higher than 84 kJ.mol^{-1} and the ΔG lower than –80 kJ.mol^{-1} [35]. The thermodynamic study was carried out at pH 7 and revealed an adsorption mechanism governed by physisorption. The same experiment carried out at pH lower than PZC would give interesting information about the prevalence of chemisorption rather than physisorption at low pH in the process studied. Physisorption is often noticed in the adsorption of P, As, and F onto metal oxides or hydroxides [36], [10] and [37].

Figure 7 The plot of ln(K_0) versus T^{-1} showing the dependency of the free energy of Gibbs to temperature

3.6 Kinetic removal of phosphorus

The kinetic study of phosphorous adsorption onto Laterite and ALS were conducted to determine the time required for the adsorption process to reach equilibrium, the effect of the particle size and the corresponding results are presented in Figure 8. Experiments were carried out at 300 rpm to eliminate the bulk diffusion resistance. It has been observed that the adsorption rate of P was quite rapid for the first 5 hours with the plateau taking place at approximately 30 hours; Figure 8 (a). However, after 48 hours, pseudo equilibrium was reached and the experiments were stopped. It can also be noticed that in the experimental conditions, the ALS material removed 80 % more than the raw Laterite material.

Figure 8: Kinetic studies of P removal (a) by raw Laterite and ALS of particle size lower than 75 µm and (b) by ALS materials of different particle sizes. Adsorbent dosage ratio is 1 g.L^{-1} and equilibrium pH is 7.0

From Figure 8 (b) it can be seen that the maximum capacity of the materials in these conditions is influenced by the particle size of the material used. There is no significant difference in the surface area of the ALS material over the particle size range studied, which could explain the difference in q_e. The slow diffusion of phosphorous and the incomplete equilibrium reached in the experiments might be responsible for the difference in q_e noticed.

Table 5 presents the parameters obtained by fitting the experimental data to the pseudo first and pseudo second order kinetics models. The pseudo first order model seems to describe more accurately the adsorption of phosphorous onto Laterite and ALS ($r^2 > 0.974$). For the pseudo first order model the values of k_1 and q_e decreased with a decrease in the ALS particle size; the smaller the particle size the quicker the adsorption rate.

Table 5: Pseudo–first and pseudo–second order kinetic model parameters

This effect is further characterized by the determination of diffusion coefficients.

3.7 Diffusion of phosphorous onto Laterite and ALS

In fact several regions can usually be noticed in the diffusion of pollutants in porous materials [27]. The presence of different regions shows the predominant resistance to diffusion of one process over another [38]. The intraparticle model assumes that the stirring speed used in the kinetic experiment is sufficient to erase the bulk liquid to solid resistance. More over this model does not differentiate between pore diffusion and surface diffusion referring to both of them as intraparticle diffusion. It is then commonly stated that the first constant region corresponds to the pore diffusion being the limit step and the second region being the surface diffusion limiting step [39, 40]. A third region can be identified in specific cases when the adsorption step is very slow [41] or because the concentration gradient is too low in the experimental conditions. When four regions are noticed this implies that the first region, corresponding to the predominance of bulk diffusion in the liquid, is a limiting mechanism in the experimental conditions. The Malash and El–Khaiary optimisation tool was used to determine the different intraparticle constants corresponding to the different diffusion stages [27].

Figure 9 presents the intraparticle diffusion model applied to the adsorption of P onto Laterite and ALS where different phases can be identified.

Figure 9 Intraparticle modelling of P removal by Laterite and ALS or particle size lower than 75 µm

In Figure 9, the plateau observed corresponds to a very slow diffusion step that can be identified as the surface diffusion step. The two other steps identified are characteristic of two

distinct intraparticle diffusion steps that can be either macropores, micropores or surface diffusion stages.

The coefficients of the different steps identified were calculated using equation (15) and are reported in Table 6. The removal of P by ALS of different diameters was modelled by two stages only, with the first one being the intraparticle diffusion stage.

Table 6 Intraparticle model coefficients for P removal by Laterite and ALS. k_{idx} refers to the coefficient of the intraparticle diffusion phase number x

The Boyd diffusion model, equation (16), fitted well the experimental data, suggesting that the diffusion was controlled by intraparticle diffusion. The Boyd coefficients and the resulting intraparticle diffusion coefficients are presented in Table 7. The values obtained for the effective diffusion coefficients are low and are characteristic of micropores to surface diffusion coefficients [42] and [43]. Diffusion coefficients in the range of 10^{-13} $m^2.s^{-1}$ to 10^{-12} $m^2.s^{-1}$ are typical values for micropore diffusion coefficients while values from 10^{-20} $m^2.s^{-1}$ to 10^{-14} $m^2.s^{-1}$ were reported for surface diffusion coefficients. The diffusion coefficients obtained for small particle diameters present values in the range of surface diffusion while particles with higher diffusion coefficients are in the range of micropore diffusion.

Table 7: Diffusion coefficient parameters of P adsorption onto ALS as a function of particle size

The diffusion of phosphorous onto ALS is mainly controlled by surface diffusion. Surface diffusion is generally the limiting step in adsorption of heavy metals onto iron, aluminium or manganese oxides [43]. The diffusion coefficients of phosphorous onto Laterite are lower than that of ALS, indicating that the surface diffusion in Laterite is slower than in ALS.

The diffusion coefficients are key data in the prediction of column breakthrough. The use of equation (20) to approximate diffusion coefficients gives a quick and good estimation method. Linear correlation between both methods is very good (i.e. 0.97) but diffusion coefficients obtained using $(k_{id1}/q_e)^2$ as approximated Boyd coefficient are underestimated by 25 %.

3.8 Adsorption – desorption mechanisms

Figure 10 presents the FTIR analysis of the ALS sample before and after adsorption of phosphate. It can be noticed that there is an increase in the 920 cm^{-1} and 946 cm^{-1} peaks in

relation to the initial phosphate concentration used in the P adsorption experiments. The 946 cm^{-1} peak is assigned to the stretching vibration mode of PO_4, and noticed in some P–Al hydroxide minerals [44]. The chemical bonding between phosphate and aluminium oxy–oxyhydroxides proves that at least part of the adsorption of phosphate onto ALS is done by chemical bonding, either chemisorption or ion–exchange.

Figure 10: FTIR analysis of P adsorption onto ALS at different starting P concentrations and comparison with raw ALS. Equilibrium time was 48 h; wavelength range is 2000 – 400 cm^{-1}

Figure 11 shows the desorption of phosphate from ALS using either NaOH or Na_2SO_4 solutions. When Na_2SO_4 solutions were used the equilibrium pHs recorded were around pH 8. The results show a maximum desorption of P from ALS at 0.1 M NaOH (pH 13), when using NaOH solutions. A slight decrease in the desorption is noticed as the NaOH concentration increases. The dissolution of SiO compounds at high pH and the possible formation of P complexes under high pH environments can explain the decrease in desorption performances.

Figure 11: Desorption of P from ALS using NaOH and Na_2SO_4 solution at different concentrations

It is interesting to note that the desorption at pH 8 using Na_2SO_4 is quite stable as the Na_2SO_4 concentration is increasing and reaches more than 33 % desorption at 0.1 M Na_2SO_4. While the NaOH desorption mechanism can rely on physical, chemical and ion–exchange desorption mechanisms, Na_2SO_4 uses only ion–exchange mechanisms to desorb P from ALS. The data presented in Figure 11 then suggests that nearly 30 % of P adsorption onto ALS can be attributed to the ion–exchange mechanism.

Table 8: DR model parameters for the isotherm of P adsorption onto ALS

Table 8 presents the parameters of the Dubinin–Radushkevich model obtained at room temperature for the adsorption of phosphate onto ALS. The determination coefficient r^2 for the application of the DR model to the data is quite low. The conclusions drawn from the analysis of the DR model parameters must then be balanced. The adsorption energy of this reaction is calculated as 5.3 $kJ.mol^{-1}$. The adsorption of phosphate onto ALS is then governed

mainly by physisorption. Nevertheless as the FTIR and desorption analysis suggested, ion–exchange is playing a role in the removal of phosphate from ALS. The adsorption of phosphorous onto ALS is therefore not a heterogeneous process. Part of it can be related to pure physical adsorption (adsorption energy < 8 $kJ.mol^{-1}$) while the other part is accounted for by ion–exchange (adsorption energy > 8 $kJ.mol^{-1}$).

4 Conclusion

The present study revealed the good phosphorus adsorption properties of the ALS material; a by–product generated during the manufacture of Ferric Aluminium Sulphate. The dosage study revealed the effect of the material and principally the remaining surface sulphate groups on the equilibrium pH and the impact on the adsorption capacity of the material. It was noticed that there is a maximum adsorption capacity at pH 5 evaluated at 3.68 mg $P.g^{-1}$ while high pHs showed a detrimental effect of OH^- groups onto phosphorus adsorption by ALS.

Moreover at an adsorbent dosage of 1 $g.L^{-1}$ the P adsorption onto the ALS material followed a Freundlich type isotherm, displaying very good removal performances at low P concentration. At 0.035 $mg.L^{-1}$, the ALS material was able to remove 1.65 mg $P.g^{-1}$.

In terms of kinetic removal, initial P adsorption onto ALS was very quick and pseudo equilibrium was reached in nearly 24 h following preferably a pseudo first order kinetic model. Nevertheless the effect of particle size on adsorption capacity kinetics revealed that equilibrium was not completely reached for bigger particles in 48 h.

Diffusion of P onto ALS was limited due to surface diffusion resistance as indicated by the mathematical modelling of the kinetic experiments. Pore and surface diffusion coefficients were determined for each particle size studied using the Boyd diffusion model. Very similar surface diffusion coefficients were obtained using the kinetic parameters, which represent a simple estimation method for modelling calibration purposes.

The desorption experiment showed a possibility of regeneration of the material for continuous applications. The capacity of this material to be used in a packed bed system or wetland type applications will be investigated under dynamic conditions.

Acknowledgement

The authors would like to thank John Kinney from Cleanfields Technologies Ltd for providing the Laterite and ALS samples. This work was performed as part of the EU

555 Framework 7 project “ATWARM” (Marie Curie ITN, No. 238273). The authors would like
556 to thank QUESTOR centre staff for their technical support.

5 References

1. McMurray, C., et al., *Report on the environmental aspects of the nitrates directive in Northern Ireland.* Department Of Environment, 2002.

2. Taylor, D., et al., *Recent histories of six productive lakes in the Irish Ecoregion based on multiproxy palaeolimnological evidence.* Hydrobiologia, 2006. **571**(1): p. 237-259.

3. Benedetti, L., *Probabilistic design and upgrade of wastewater treatment plants in the EU Water Framework Directive context*, 2006, Ghent University.

4. Mainstone, C.P. and W. Parr, *Phosphorus in rivers — ecology and management.* Science of The Total Environment, 2002. **282–283**: p. 25-47.

5. Barca, C., et al., *Phosphate removal from synthetic and real wastewater using steel slags produced in Europe.* Water Research, 2012. **46**(7): p. 2376-2384.

6. Gao, S., C. Wang, and Y. Pei, *Comparison of different phosphate species adsorption by ferric and alum water treatment residuals.* Journal of Environmental Sciences, 2013. **25**(5): p. 986-992.

7. Huang, W., et al., *Phosphate removal from wastewater using red mud.* Journal of Hazardous Materials, 2008. **158**(1): p. 35-42.

8. Liu, C.-j., et al., *Adsorption removal of phosphate from aqueous solution by active red mud.* Journal of Environmental Sciences, 2007. **19**(10): p. 1166-1170.

9. Vohla, C., et al., *Filter materials for phosphorus removal from wastewater in treatment wetlands—A review.* Ecological Engineering, 2011. **37**(1): p. 70-89.

10. Glocheux, Y., et al., *Removal of arsenic from groundwater by adsorption onto an acidified laterite by-product.* Chemical Engineering Journal, 2013.

11. Hill, I.G., R.H. Worden, and I.G. Meighan, *Geochemical evolution of a palaeolaterite: the Interbasaltic Formation, Northern Ireland.* Chemical Geology, 2000. **166**(1-2): p. 65-84.

12. Tsang, S., et al., *Determination of phosphate/arsenate by a modified molybdenum blue method and reduction of arsenate by S2O42−.* Talanta, 2007. **71**(4): p. 1560-1568.

13. Limousin, G., et al., *Sorption isotherms: A review on physical bases, modeling and measurement.* Applied Geochemistry, 2007. **22**(2): p. 249-275.

14. Gérente, C., et al., *Removal of arsenic(V) onto chitosan: From sorption mechanism explanation to dynamic water treatment process.* Chemical Engineering Journal, 2010. **158**(3): p. 593-598.

15. Hamdaoui, O. and E. Naffrechoux, *Modeling of adsorption isotherms of phenol and chlorophenols onto granular activated carbon: Part I. Two-parameter models and equations allowing determination of thermodynamic parameters.* Journal of Hazardous Materials, 2007. **147**(1–2): p. 381-394.

16. Hutson, N.D. and R.T. Yang, *Theoretical basis for the Dubinin-Radushkevitch (DR) adsorption isotherm equation.* Adsorption, 1997. **3**(3): p. 189-195.

17. Dada, A., et al., *Langmuir, Freundlich, Temkin and Dubinin–Radushkevich Isotherms Studies of Equilibrium Sorption of Zn 2 Unto Phosphoric Acid Modified Rice Husk.* IOSR Journal of Applied Chemistry, 2012. **3**(1): p. 38-45.

18. Al-Anber, M., *Thermodynamics Approach in the Adsorption of Heavy Metals.* Juan Carlos Moreno-Pirajan, Thermodynamics-Interaction Studies-Solids, Liquids and Gases Book, first ed., In-Tech, Rijeka, 2011: p. 737-764.

19. Lagergren, S., *About the theory of so-called adsorption of soluble substances.* Kungliga Svenska Vetenskapsakademiens Handlingar, 1898. **24**(4): p. 1-39.

20. Ho, Y.S. and G. McKay, *Pseudo-second order model for sorption processes.* Process Biochemistry, 1999. **34**(5): p. 451-465.

21. Niwas, R., et al., *The adsorption of phosphamidon on the surface of styrene supported zirconium (IV) tungstophosphate: a thermodynamic study.* Colloids and Surfaces A: Physicochemical and Engineering Aspects, 2000. **164**(2–3): p. 115-119.

22. Ramesh, A., D.J. Lee, and J.W.C. Wong, *Thermodynamic parameters for adsorption equilibrium of heavy metals and dyes from wastewater with low-cost adsorbents.* Journal of Colloid and Interface Science, 2005. **291**(2): p. 588-592.

23. Aksu, Z., *Determination of the equilibrium, kinetic and thermodynamic parameters of the batch biosorption of nickel(II) ions onto Chlorella vulgaris.* Process Biochemistry, 2002. **38**(1): p. 89-99.

24. Huang, X., N.-y. Gao, and Q.-l. Zhang, *Thermodynamics and kinetics of cadmium adsorption onto oxidized granular activated carbon.* Journal of Environmental Sciences, 2007. **19**(11): p. 1287-1292.

25. Milonjic, S., *A consideration of the correct calculation of thermodynamic parameters of adsorption.* Journal of the Serbian Chemical Society, 2007. **72**(12): p. 1363-1367.

26. Weber, W.J. and J.C. Morris, *Kinetics of adsorption on carbon from solution.* J. Sanit. Eng. Div. Am. Soc. Civ. Eng, 1963. **89**(17): p. 31-60.

27. Malash, G.F. and M.I. El-Khaiary, *Piecewise linear regression: A statistical method for the analysis of experimental adsorption data by the intraparticle-diffusion models.* Chemical Engineering Journal, 2010. **163**(3): p. 256-263.

28. Reichenberg, D., *Properties of Ion-Exchange Resins in Relation to their Structure. III. Kinetics of Exchange.* Journal of the American Chemical Society, 1953. **75**(3): p. 589-597.

29. Morin, W. and P.C. Todor, *Laterite and lateritic soils and other problem soils of the tropics*. 1979: IPR, 1979. cap. 7 e 8.

30. Meenakshi, S., C.S. Sundaram, and R. Sukumar, *Enhanced fluoride sorption by mechanochemically activated kaolinites.* Journal of Hazardous Materials, 2008. **153**(1–2): p. 164-172.

31. He, L.M., et al., *Ionic Strength Effects on Sulfate and Phosphate Adsorption on γ-Alumina and Kaolinite: Triple-Layer Model.* Soil Science Society of America Journal, 1997. **61**(3).

32. Toth, J., *Adsorption*. 2002: CRC Press. 904.

33. Albadarin, A.B., et al., *Influence of solution chemistry on Cr(VI) reduction and complexation onto date-pits/tea-waste biomaterials.* Journal of Environmental Management, 2013. **114**: p. 190-201.

34. Demiral, H., et al., *Adsorption of chromium(VI) from aqueous solution by activated carbon derived from olive bagasse and applicability of different adsorption models.* Chemical Engineering Journal, 2008. **144**(2): p. 188-196.

35. Kuo, C.-Y., C.-H. Wu, and J.-Y. Wu, *Adsorption of direct dyes from aqueous solutions by carbon nanotubes: Determination of equilibrium, kinetics and thermodynamics parameters.* Journal of Colloid and Interface Science, 2008. **327**(2): p. 308-315.

36. Rodrigues, L.A. and M.L.C.P. da Silva, *An investigation of phosphate adsorption from aqueous solution onto hydrous niobium oxide prepared by co-precipitation method.* Colloids and Surfaces A: Physicochemical and Engineering Aspects, 2009. **334**(1–3): p. 191-196.

37. Tomar, V. and D. Kumar, *A critical study on efficiency of different materials for fluoride removal from aqueous media.* Chemistry Central Journal, 2013. **7**(1).

38. Wu, F.-C., R.-L. Tseng, and R.-S. Juang, *Kinetic modeling of liquid-phase adsorption of reactive dyes and metal ions on chitosan.* Water Research, 2001. **35**(3): p. 613-618.

39. Albadarin, A.B., et al., *Kinetic and thermodynamics of chromium ions adsorption onto low-cost dolomite adsorbent.* Chemical Engineering Journal, 2012. **179**: p. 193-202.

40. Rengaraj, S., et al., *Adsorption characteristics of Cu(II) onto ion exchange resins 252H and 1500H: Kinetics, isotherms and error analysis.* Journal of Hazardous Materials, 2007. **143**(1–2): p. 469-477.

41. Zhang, J. and R. Stanforth, *Slow Adsorption Reaction between Arsenic Species and Goethite (α-FeOOH): Diffusion or Heterogeneous Surface Reaction Control.* Langmuir, 2005. **21**(7): p. 2895-2901.

42. Crini, G. and P.-M. Badot, *Sorption processes and pollution: Conventional and non-conventional sorbents for pollutant removal from wastemasters*. 2010: Presses Univ. Franche-Comté. 500.

43. Axe, L. and P. Trivedi, *Intraparticle Surface Diffusion of Metal Contaminants and their Attenuation in Microporous Amorphous Al, Fe, and Mn Oxides.* Journal of Colloid and Interface Science, 2002. **247**(2): p. 259-265.

44. Roncal-Herrero, T., et al., *Precipitation of iron and aluminum phosphates directly from aqueous solution as a function of temperature from 50 to 200 °C.* Crystal Growth & Design, 2009. **9**(12): p. 5197-5205.

45. Jellali, S., et al., *Adsorption characteristics of phosphorus from aqueous solutions onto phosphate mine wastes.* Chemical Engineering Journal, 2011. **169**(1–3): p. 157-165.

46. Sakadevan, K. and H.J. Bavor, *Phosphate adsorption characteristics of soils, slags and zeolite to be used as substrates in constructed wetland systems.* Water Research, 1998. **32**(2): p. 393-399.

47. Moharami, S. and M. Jalali, *Removal of phosphorus from aqueous solution by Iranian natural adsorbents.* Chemical Engineering Journal, 2013. **223**: p. 328-339.

Table 9 XRD analysis of raw Laterite and ALS samples. Results are expressed in % w/w

Crystal	Formula	Laterite	ALS
Gibbsite	$Al(OH)_3$	72.1	60.5
Anatase	TiO_2	2.0	2.4
Hematite	Fe_2O_3	1.9	2.4
Magnetite	Fe_3O_4	7.3	7.4
Kaolinite	$Al_2Si_2O_5(OH)_4$	16.7	27.3

Table 10 Isotherm models parameters and correlation coefficient of P adsorpiton onto ALS

	Langmuir isotherm			Freundlich isotherm		
Parameters	q_m (mg.g^{-1})	b_L (L.mg^{-1})	r^2	K_f(mg^{1-n}.g^{-1}.L^n)	n	r^2
ALS adsorbent	2.730	1.460	0.923	2.090	0.070	0.980

Table 11 Comparison of P adsorption capacities of ALS and reported results from the literature

Adsorbents	Removal capacity in mg P.g^{-1}	Best fit isotherm	Reference
Phosphate mine wastes	8.70	Freundlich	[45]
Zeolite	2.15	Freundlich	[46]
Blast furnace slag	0.44	Freundlich	[46]
Calcite	1.82	Freundlich	[47]
Acidified Laterite by–product	2.73	Freundlich	This Study

Table 12 Free energy of Gibbs, enthalpy and entropy of P adsorption onto ALS

Temperature	ΔG (kJ.mol^{-1})	ΔH (kJ.mol^{-1})	ΔS (J.mol^{-1}.K^{-1})
298 K	–10.06	5.54	52.37
303 K	–10.32		
313 K	–10.82		
323 K	–11.38		

Table 13: Pseudo–first and pseudo–second order kinetic model parameters

		Pseudo first order			Pseudo second order		
	Particle diameter	k_1	q_e	r^2	k_2	q_e	r^2
Adsorbent	µm	h^{-1}	mg.g^{-1}		g.mg^{-1}.h^{-1}	mg.g^{-1}	
Laterite	< 75	0.383	1.487	0.991	0.356	1.630	0.986
ALS	< 75	0.271	2.668	0.997	0.126	2.923	0.992
ALS	500 – 600	0.224	2.245	0.974	0.104	2.532	0.965
ALS	1000 – 1180	0.182	1.693	0.989	0.105	1.944	0.980

Table 14 Intraparticle model coefficients for P removal by Laterite and ALS. k_{idx} refers to the coefficient of the intraparticle diffusion phase number x

	Particle diameter	Intraparticle diffusion coefficients in mg.g^{-1}.h$^{-0.5}$					
Adsorbent	µm	k_{id1}	r^2	k_{id2}	r^2	k_{id3}	r^2
Laterite	< 75	0.589	0.996	0.425	0.981	0.026	0.882
ALS	< 75	0.885	0.994	0.083	1.000	–	–
ALS	500 – 600	0.717	0.931	0.146	1.000	–	–
ALS	1000 – 1180	0.480	0.934	0.063	1.000	–	–

Table 15: Diffusion coefficient parameters of P adsorption onto ALS as a function of particle size

Sorbent	$Ø_{median}$	B ($\times 10^{-2}$)	D_{eff} ($\times 10^{-13}$)	$(k_{id1}/q_e)^2$ ($\times 10^{-2}$)	D_{eff} ($\times 10^{-13}$)
	µm	min^{-1}	$m^2.s^{-1}$	min^{-1}	$m^2.s^{-1}$
Laterite	37.5	0.364	0.021	0.261	0.016
ALS	37.5	0.575	0.034	0.453	0.027
ALS	550	0.236	3.013	0.170	2.170
ALS	1090	0.202	10.10	0.134	6.730

The diffusion of phosphorous onto ALS is mainly controlled by surface diffusion. Surface

Table 16: DR model parameters for the isotherm of P adsorption onto ALS

Adsorbent	Pollutant	pH_e	q_s	k_{ad}	r^2	E
			$mg.g^{-1}$	$mol^2.kJ^{-2}$		$kJ.mol^{-1}$
ALS	P	7	2.55	18.15	0.845	5.26

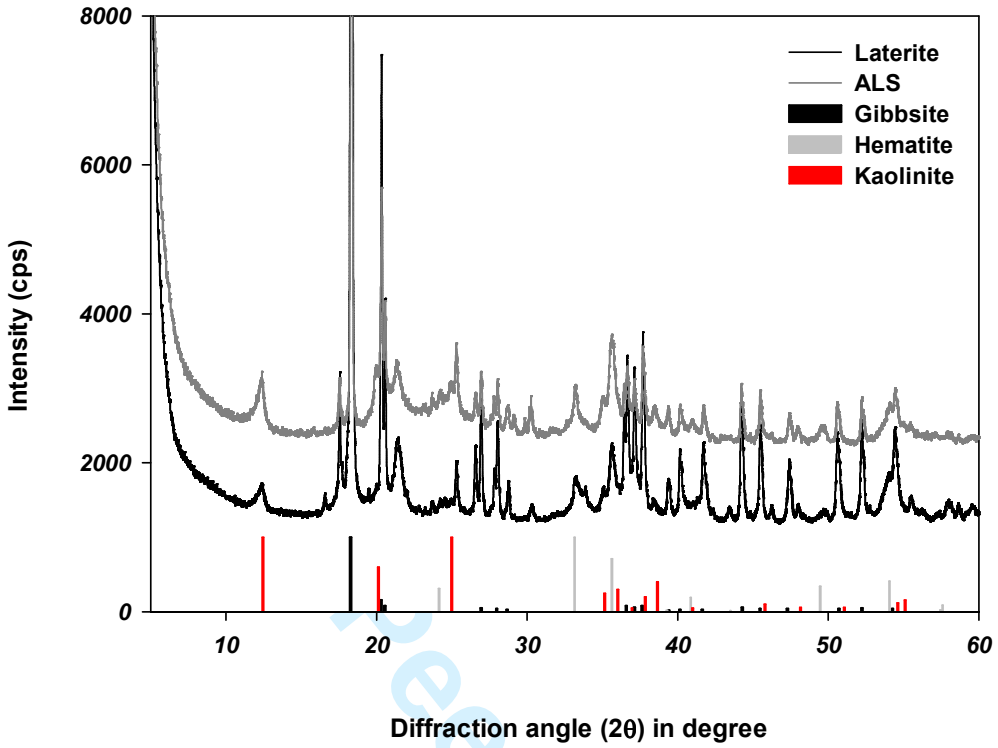

Figure 1 XRD spectrum of laterite and ALS samples and main crystals phases identified

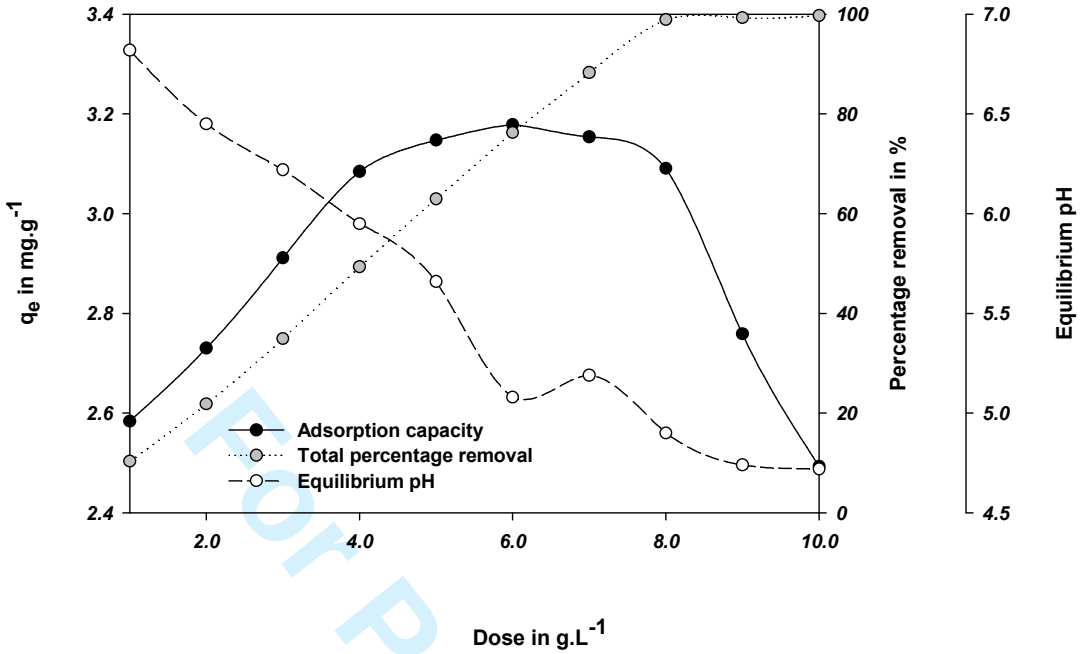

Figure 2 Phosphorus removal by increasing ALS dosage ratio; $[P]_0 \approx 25$ ppm; pH_0 is 7

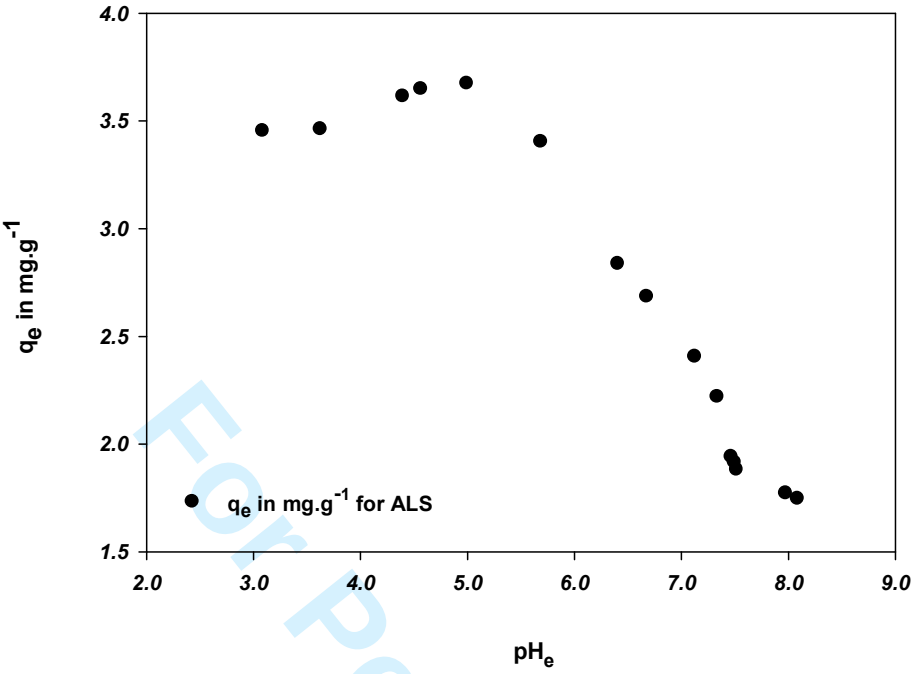

Figure 3 Phosphorus adsorption study in function of pH at equilibrium. $[P]_0 \approx 25$ ppm

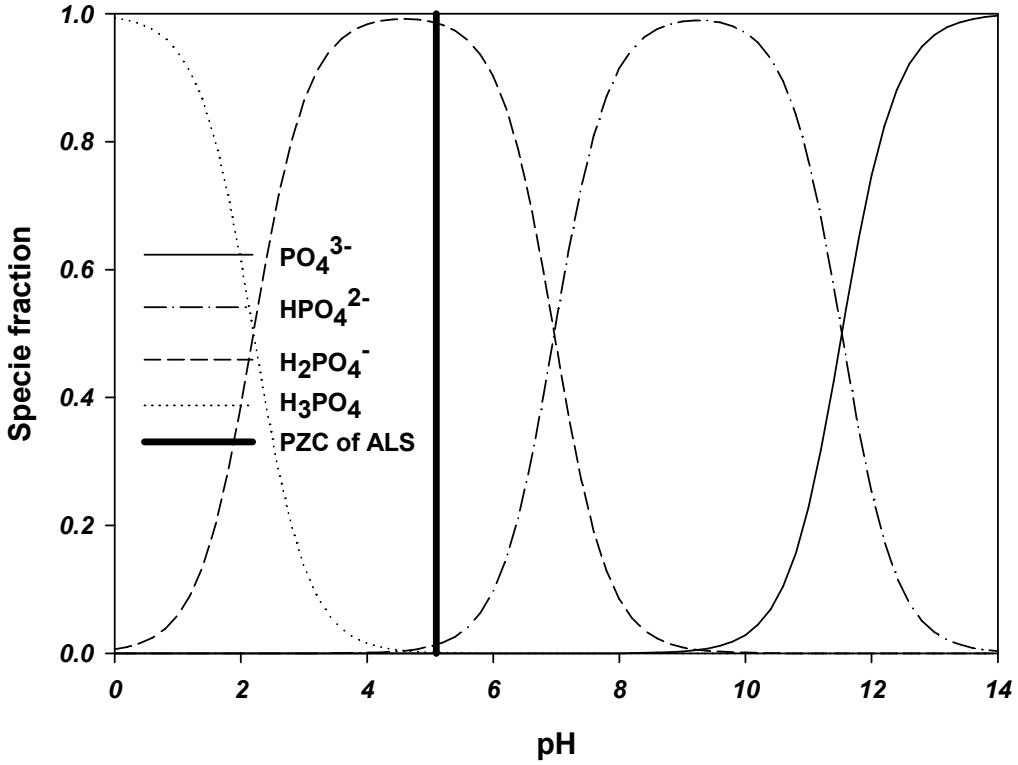

Figure 4 Phosphorous speciation diagram and PZC of the lateritic by□product ALS

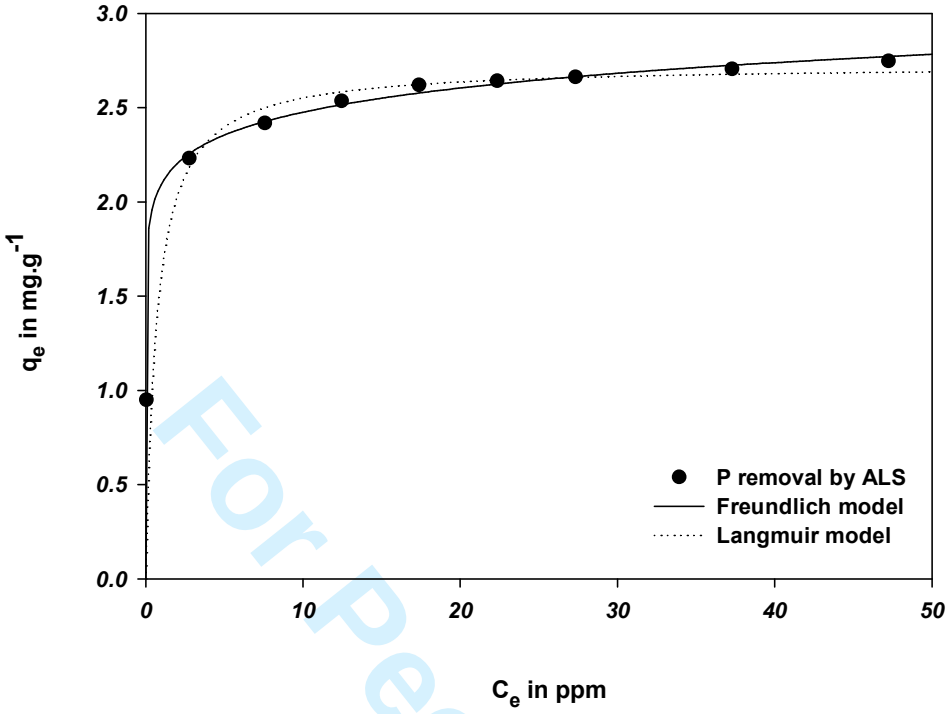

Figure 5 Isotherm modelling of phosphorus adsorption onto ALS. ALS particle size is lower than 75 µm and $pH_e \approx 7.0$

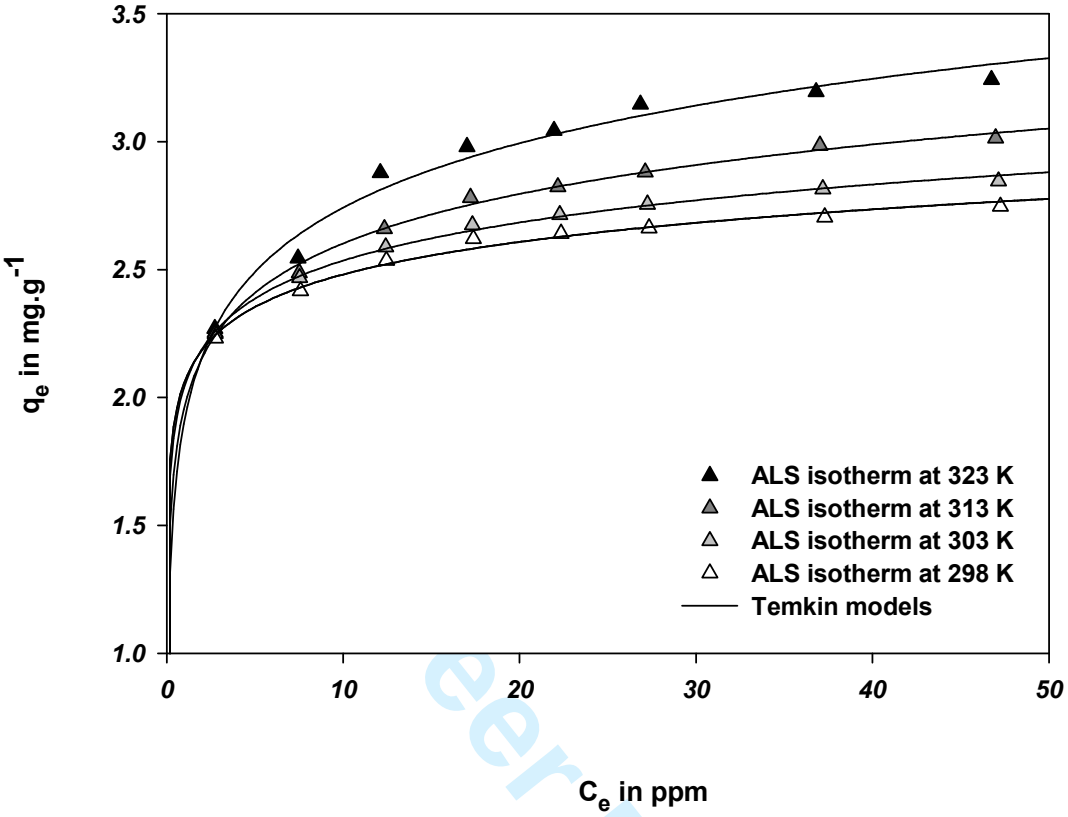

Figure 6 P adsorption isotherms obtained at different temperature modelled using Temkin isotherm mathematical model

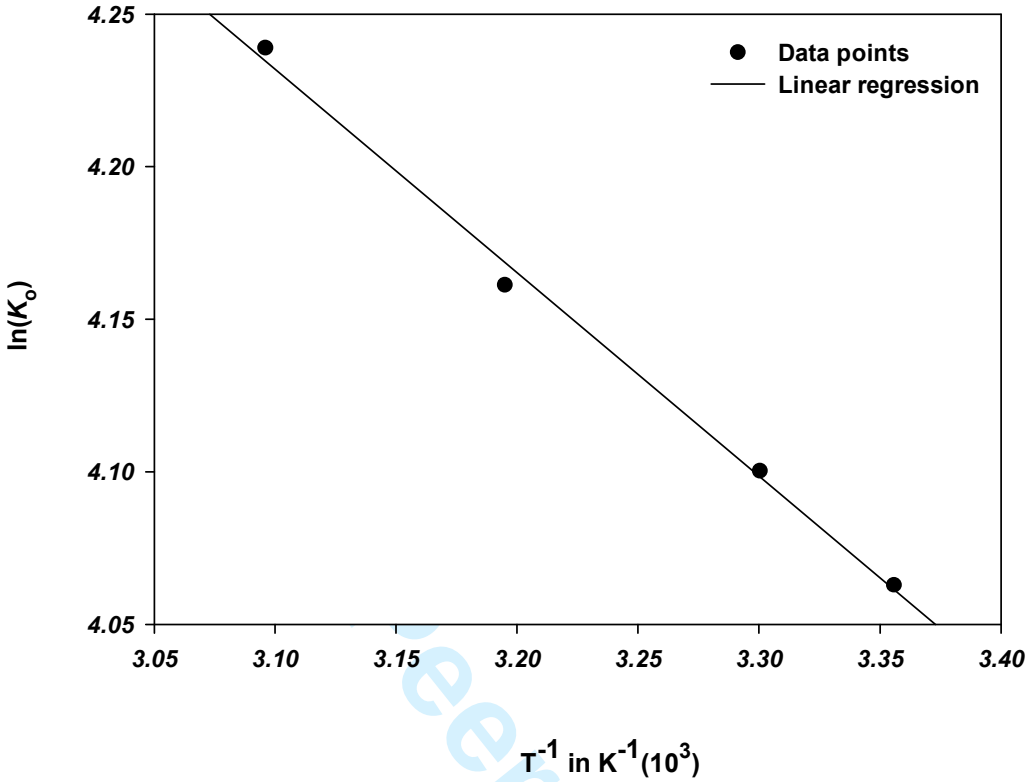

Figure 7 The plot of $\ln(K_0)$ versus T^{-1} showing the dependency of the free energy of Gibbs to temperature

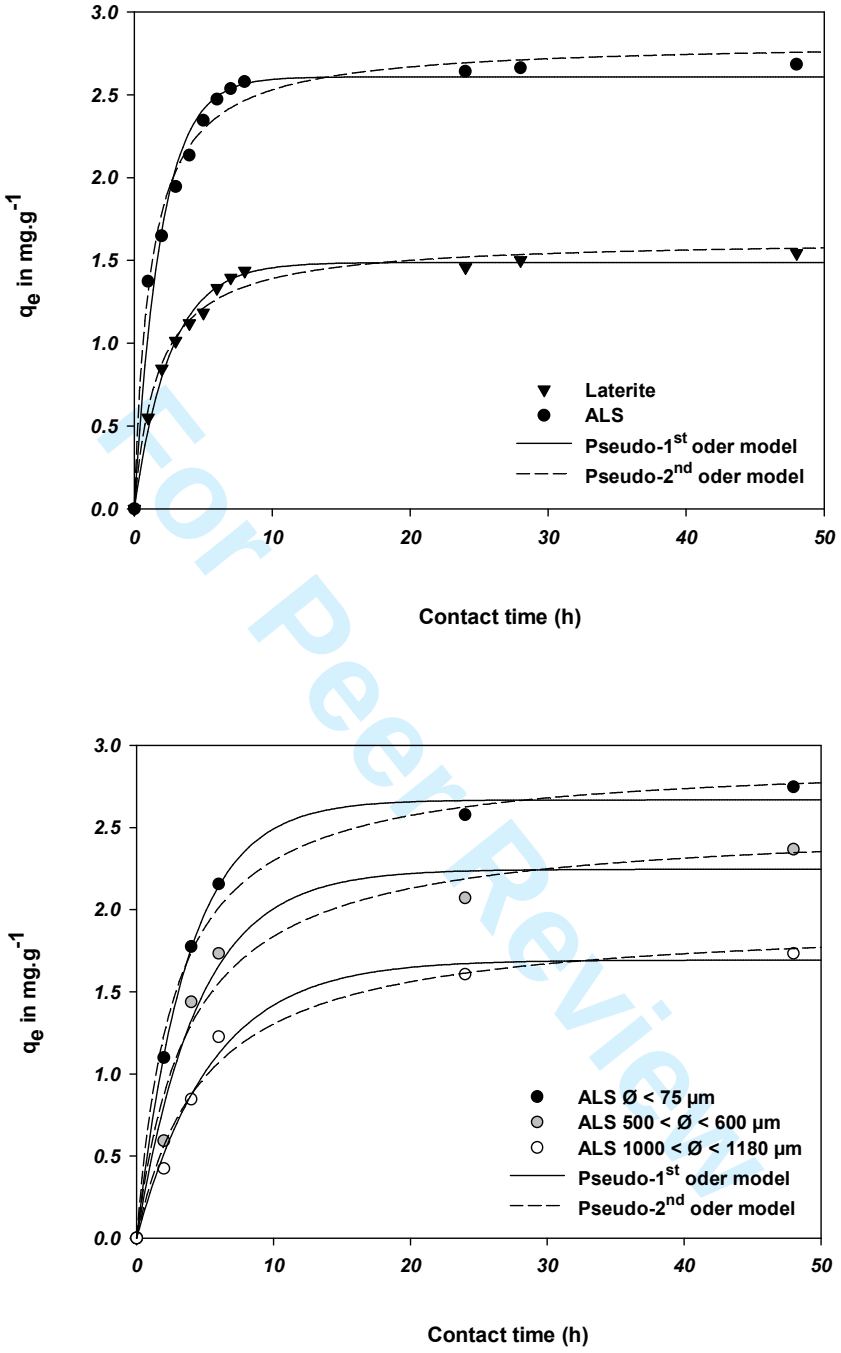

Figure 8 Kinetic studies of P removal (a) by raw laterite and ALS of particle size lower than 75 µm and (b) by ALS materials of different particle sizes. Adsorbent dosage ratio is 1 g.L^{-1} and equilibrium pH is 7.0

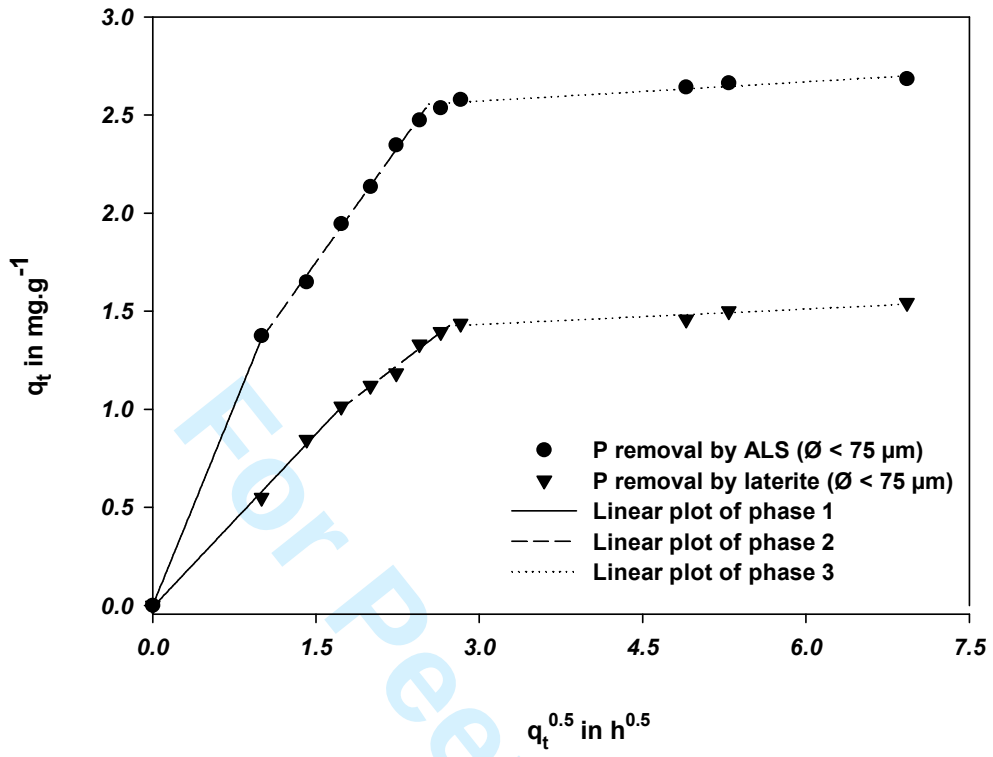

Figure 9 Intraparticle modelling of P removal by laterite and ALS or particle size lower than 75 µm

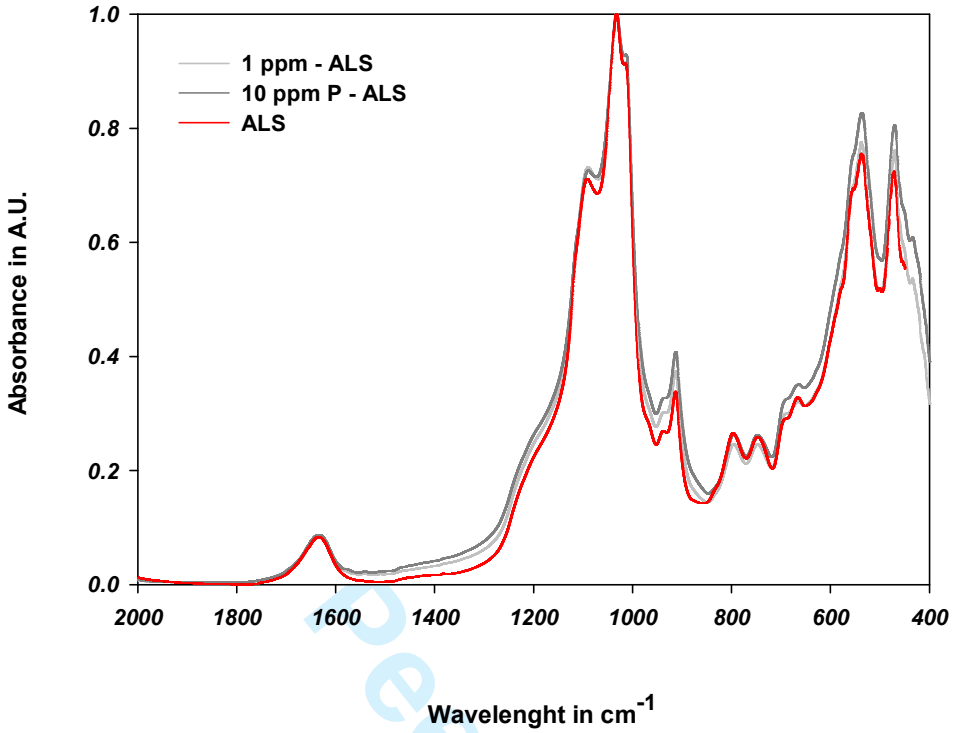

Figure 10 FTIR analysis of P adsorption onto ALS at different starting P concentration and comparison with raw ALS. Equilibrium time was 48 h, wavelength range is 2000 □ 400 cm□1

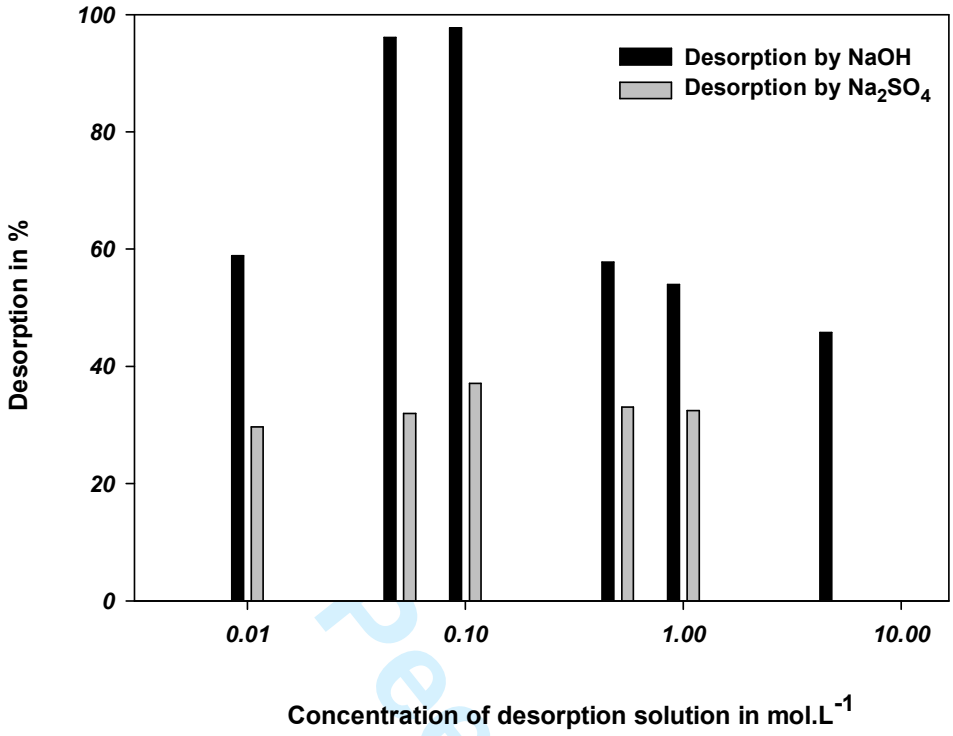

Figure 11 Desorption of P from ALS using NaOH and Na_2SO_4 solution at different concentration